Susceptibility of the two-dimensional electron gas: Diamagnetic spikes and gaps in the density of states

R. S. Markiewicz, M. Meskoob, and B. Maheswaran
Department of Physics, Northeastern University, Boston, Massachusetts 02115
and Francis Bitter National Magnet Laboratory, Massachusetts Institute of Technology, Cambridge, Massachusetts 02139
(Received 9 January 1987)

In a strong magnetic field, Br_2-graphite intercalation compounds behave as nearly ideal two-dimensional (2D) hole gases, with nonoverlapping Landau levels, leading to large diamagnetic spikes in the susceptibility. These spikes are broadened by sample inhomogeneities, corresponding to $\sim 0.4\%$ density fluctuations. As a byproduct of the analysis, some general features of the 2D susceptibility are clarified.

I. INTRODUCTION

In an intense magnetic field, the energy bands of a two-dimensional electron gas (2D EG) are split into a series of Landau levels:

$$E_N=(N+\tfrac{1}{2})\hbar\omega_c \ ,$$

where N is an integer ≥ 0, $\omega_c=eB/mc$ is the cyclotron frequency, and m is the effective carrier mass. Ideally, all the states within a Landau level are degenerate in energy, and separated from the next Landau level by a gap, $\hbar\omega_c$. In reality, the levels are broaded by disorder, sample inhomogeneity, and effects of three dimensionality, and it has proven to be extremely difficult to observe this gap. Even in samples which display the quantum Hall effect[1] (QHE) a number of very careful experiments[2–8] have shown that the density of states between Landau levels remains a significant fraction of the zero-field density of states. Fortunately, all that is necessary for observation of the QHE is a *mobility gap* and not a true energy gap, and disorder easily localizes states away from the Landau level center.

In this paper evidence is presented for the first observation of a true energy gap between Landau levels in a 2D EG. In this case the carrier gas (actually a hole gas) is formed in a graphite intercalation compound (GIC).[9] Hence bulk ($\sim$1-mm-thick) samples may easily be formed, in contrast to the QHE materials, which are typically only a few hundred Å's thick. This affords a tremendous advantage in probing thermodynamic properties of the 2D EG. While the high carrier density makes it improbable that a QHE will be observed, new phenomena have been predicted[10] which may involve a magnetic analog of the QHE.[11] A critical question is whether the electron gas in GIC behaves two dimensionally, or whether interlayer coupling broadens the Landau levels to such an extent that they always overlap. The bandwidth in the direction perpendicular to the layers ("c-axis" dispersion) has recently been estimated from the conductivity anisotropy,[12] and it is found that many acceptor compounds should be in the 2D limit. The present work provides a detailed analysis of ac susceptibility ($\chi=dM/dB$) oscillations in a Br_2-GIC. Evidence is presented that, despite the high carrier density ($n\cong 10^{14}$ cm^{-2}) and large sample thickness ($\sim$1 mm), the Landau levels are extremely sharp (full width is equal to $2\Gamma\cong 3$ meV) and hence well separated in strong fields. The susceptibility displays the large negative spikes, but smeared out by residual sample inhomogeneity.

II. MATERIAL PROPERTIES

Br_2 is intercalated into plates of highly oriented pyrolytic graphite (HOPG) either by a standard two bulb technique[9] or by direct immersion of the HOPG in Br_2 liquid. The final product is stage 2—two graphite layers per intercalant layer. A representative group of samples was analyzed by (00l)-x-ray diffraction and all were found to be pure stage 2. This is consistent with the de Haas–van Alphen (dHvA) oscillations themselves, which showed only two fundamental high-frequency oscillations, characteristic of the two hole Fermi surfaces, plus harmonic and mixing frequencies. A single additional low frequency, observed in many samples, has not been positively identified.

The 2D hole gas is confined to the two graphite layers, 6.7-Å thick and separated from the next graphite layer by the 3.7 Å-thick Br_2 layer. A stage 2 sample has two hole bands—light and heavy holes. Their characteristic parameters, dHvA frequency, and effective mass, are listed in Table I. The characteristic frequencies F have been determined by Fourier transforming the dHvA spectra (which are periodic in $1/B$), while the light-hole mass is determined from the temperature dependence of the dHvA amplitudes. The heavy-hole mass could only be approximately estimated in this fashion, and the entry in Table I is a theoretical value[13] (Appendix A) consistent with measurements. (The experimental and theoretical light-hole masses are in good agreement.)

Appendix A offers a brief summary of the band structure, including calculations of the Fermi energy, effective masses, and c-axis dispersion. The bands are highly nonparabolic, but it is shown that the magnetization is the

TABLE I. Hole parameters.

	Light holes	Heavy holes
dHvA frequency F (T)	262	900
2D carrier density n (cm^{-2})	2.6×10^{13}	9.0×10^{13}
effective mass m/m_0	0.11 (0.127)[a]	(0.252)[a]
level broadening Γ (meV)	1.4	1.4
B_{2D} (T), from Eq. (7)	2.6	5.6

[a]Theoretical value, see Appendix A.

same as that for parabolic bands, if the correct effective masses are used, and if the Fermi levels are adjusted to give the correct values of F.

III. EXPERIMENTAL PROCEDURE

Since Br_2-GIC will deintercalate unless maintained in an atmosphere of excess Br_2, extreme care must be taken in handling the samples. Hence the sample is sealed in a glass ampoule, and the susceptibility is measured inductively, using a weak-field modulation technique. The sample is mounted inside two concentric copper coils. An ac voltage at frequency $\omega/2\pi$ is fed into the outer drive coil producing a time-varying magnetic field which excites magnetization oscillations in the sample. These magnetization oscillations are detected by the second pickup coil. This pickup coil is in series with a balance coil, wound with the opposite helicity. Their coupling to the drive coil can be adjusted so that there is essentially no net pickup signal (<1 μV) when the sample is removed. The output of the pickup coil, with sample inserted, is amplified and fed into a two-phase lock-in detector. At sufficiently low frequencies, the out-of-phase signal is proportional to $\omega\chi$, while the in-phase signal (which is quadratic in ω) is a combination of χ and resistivity ρ. The temperature dependence is weak in the temperature range studied (1.5–4.2 K). Figure 1 shows typical susceptibility data from a number of samples. The differences between the various spectra are predominantly due to small sample-to-sample variations of dHvA frequencies, as comparison with theory (Fig. 2) shows. However, only Fig. 1(b) is at low frequency ($\omega/2\pi=241$ Hz) to allow straightforward correction for eddy current effects. At this frequency, the corrections are small, and the corrected spectrum [Fig. 1(b)] essentially identical to one taken at 81 Hz, except for improved signal-to-noise ratio. While the shape of the oscillations is correctly given by theory, our estimate of

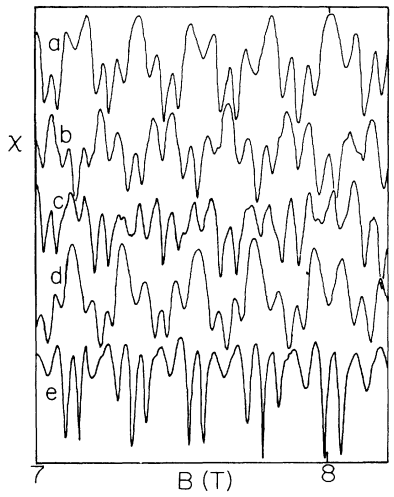

FIG. 1. dHvA spectra of five samples of Br_2-GIC, constrained from vibrating in different ways: (a) and (e): held in place with glass wool; (b): in liquid Br_2; (c): In tight-fitting glass ampoule; and (d): with pressure contacts for resistivity measurements. Zeroes of successive spectra have been shifted to avoid overlap.

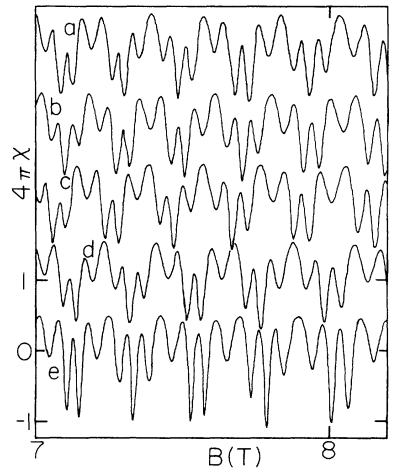

FIG. 2. Theoretical dHvA spectra corresponding to Fig. 1. All spectra have the same values of $\Gamma_h=1.4$ meV, $\Gamma_l=1.4$ meV, and Gaussian broadening with variance $\sigma/n=0.0015$ [except for (e), with $\sigma/n=0.0010$]. These spectra differ only in the values of dHvA frequencies, which were taken from Fourier transform spectra except as noted: (a): $F_l=270$ T, $F_h=921$ T; (b): 270 T, 902 T; (c): 269 T, 890 T; (d): 264 T (262.5 T from Fourier transform), 886.5 T; (e): 257 T, 880 T.

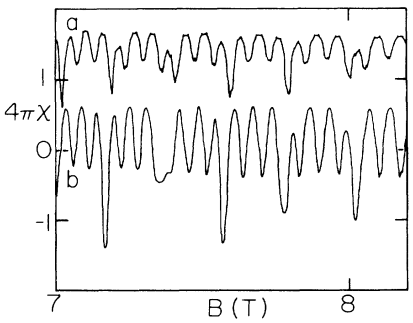

FIG. 3. Theoretical dHvA spectra based on alternative models to Fig. 2: (a) $\Gamma_l=\Gamma_h=0.5B$ meV (with B in T) (no Gaussian broadening); (b) no interband transitions—i.e., light- and heavy-hole Fermi levels independently held constant. Same Γ values and Gaussian broadening as in Fig. 2.

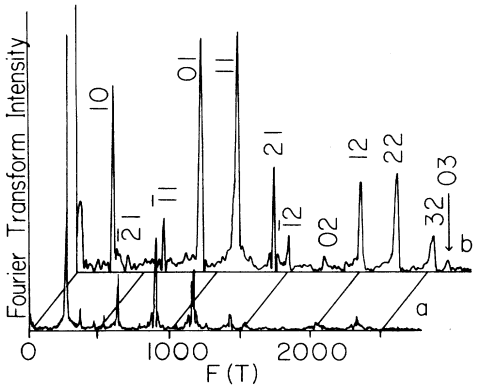

FIG. 4. Fourier transform (in $1/B$) of dHvA spectra. (a) Same sample as Fig. 1(b), transformed over range 2–15 T; (b) same sample as Fig. 1(e), transformed over range 7–15 T. All peaks can be indexed as $mF_l + nF_h$, where the integers m and n are listed in the figure (a bar over the m means m is negative).

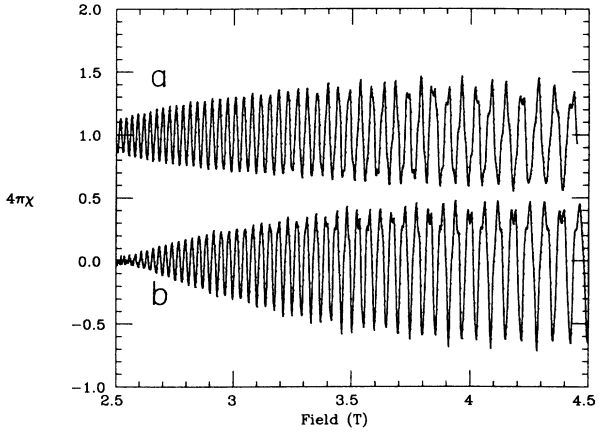

FIG. 6. Extension of Fig. 5 to lower fields.

the amplitudes of the oscillations is somewhat lower than predicted, typically by a factor of 2 or 3. This is briefly discussed in Appendix B, along with our method of calibrating the amplitude. A future publication will discuss the questions of amplitude and eddy current corrections in more detail.

The two-coil susceptometer allows considerable flexibility in sample handling, and a number of mounting arrangements were studied. Initially the samples were sealed in the glass ampoules in which they had been intercalated, with an excess of Br_2 gas. The samples were typically 1 cm$\times$1 cm$\times$0.7 mm (after intercalation), and were pressed flat against the bottom of the ampoule (perpendicular to the field B) by a pad of glass wool. While this procedure worked on occasion [Figs. 1(a) and 1(e)], in other samples the glass wool failed to provide sufficient sample rigidity. In these samples the strong magnetic torque led to significant sample motion, causing a torque instability[14] which greatly distorted the χ oscillations and introduced a hysteresis. (These effects greatly resemble strong magnetic interactions, and were initially mistaken for that effect.[15]) More rigid mountings were introduced, which eliminated these undesirable effects. There is a danger that these rigid mounts can strain the sample and distort the data, but three different mounting techniques were utilized, and all gave essentially the same $\chi(B)$ curves. These techniques were (1) remove the sample from its glass ampoule and mount in a rigid press. The press included pressure contacts for measurements of resistivity and Hall effect, and could be mounted inside the susceptometer. The sample was mounted under liquid N_2 to reduce problems of deintercalation. With care, samples prepared this way could have dHvA oscillations as sharp [Fig. 1(d)] as those prepared by other techniques, but often the oscillations showed considerably greater smearing. (2) Mount the sample in a glass ampoule of rectangular cross section, where the thickness just matches the (intercalated) sample thickness [Fig. 1(c)]. (3) Intercalate the sample by direct immersion into liquid Br_2, and seal off the im-

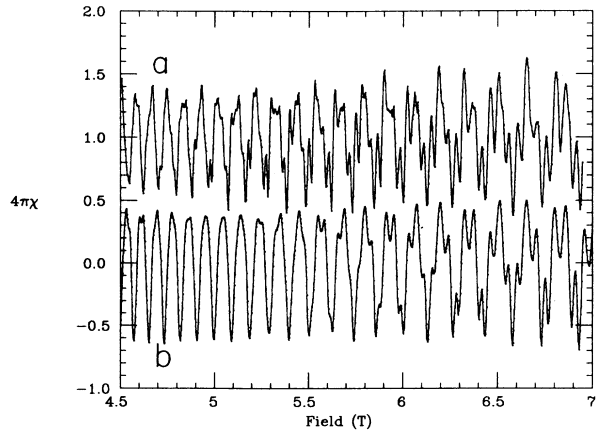

FIG. 5. Lower field comparison of experiment (a) and theory (b), for sample (b) of Figs. 1 and 2. To facilitate comparison, experimental data have been shifted down by 0.05 T, and their amplitude multiplied by 3 (see Appendix B).

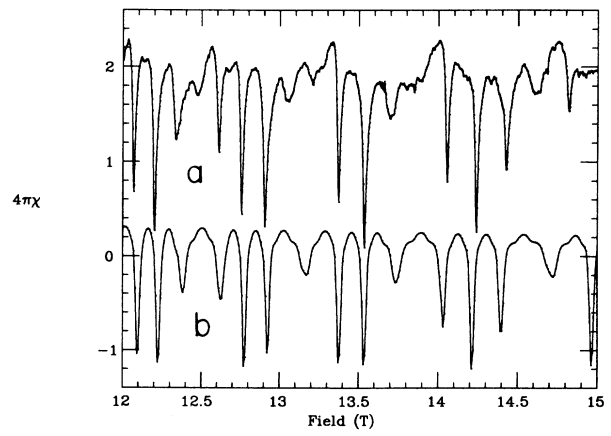

FIG. 7. High field comparison of experiment (a) to theory (b), for sample (e) of Figs. 1 and 2. These are the sharpest spikes we have so far observed.

mersed sample [Fig. 1(d)]. When cooled, the frozen Br_2 effectively clamps the sample. Direct immersion is believed to produce a slightly different in-plane superlattice of the Br_2 atoms from the usual gas phase intercalation, but no significant differences were observed in the de Haas-van Alphen spectrum of χ.

The most striking feature of Fig. 1 is the presence of two distinct periodicities, as expected for a stage 2 GIC. It is clear that the susceptibility cannot be written simply as a superposition of two independent oscillations [compare Fig. 3(b)]. A Fourier transform of the spectrum (Fig. 4) confirms this—there are strong peaks corresponding to sum and difference frequencies of the two F's. The theory described below readily explains the interference effects (Figs. 2, 5–7)—they are due to interband hole transitions. Only the total number of holes is fixed, and to keep a common Fermi level, holes must be continually interchanged between the two bands as the magnetic field is varied. This will be discussed more fully in the following section.

IV. SUSCEPTIBILITY LINE SHAPE

A. Ideal 2D EG

At temperature $T=0$ K, in the absence of impurities, each Landau level is a δ function in energy, having a degeneracy per unit area of B/Φ_0 where $\Phi_0=hc/e$ (spin and orbital degeneracy will not be considered until Sec. IV D). In this idealized case, the magnetization M has a sawtooth shape as a function of field, and $\chi=dM/dB$ has negative spikes when M changes discontinuously. The electronic energy ε and its derivatives (at $T=0$), $M=-\partial\varepsilon/\partial B$, and χ are all periodic in $1/B$, the period being $F=n\Phi_0$, where n is the (2D) electron density. The fields $B_N=F/N$ correspond to having exactly N filled Landau levels. Between these fields ε varies quadratically with B, so M is linear in B and χ is constant. At the fields B_N, M decreases discontinuously, giving χ its sharp negative spike. The negative spikes show up particularly clearly in the high field range, Fig. 7.

B. Broadening

In comparing these predictions to experimental data, the challenge is to understand how the ideal results are modified by complicating factors, such as disorder, interaction, and finite temperature. Disorder and interaction will broaden the Landau levels, giving them a finite density of states over an extended energy range about E_N. However, as long as successive Landau levels do not overlap, M will have a discontinuity and χ a spike. Vagner and Maniv[16] have shown that finite temperature eliminates the discontinuity in M, but for low temperatures the jump in M is still extremely sharp, so that large, but finite, spikes remain in χ. These same authors showed that a density of localized states within the gap between Landau levels will gradually eliminate the spike in χ. However, this spike is extremely sensitive to gross sample inhomogeneities. A variation in carrier density, for instance, will cause the spike to occur at different fields in different parts of the sample, thereby producing a very broadened dip in χ.

C. Line-shape calculation—macroscopic inhomogeneity

Once the band parameters are known (F,m), the susceptibility line shape is determined by the various broadening parameters. Since χ is approximately T independent at these low temperatures, the $T=0$ limit can be taken. In the present problem there are two principle types of broadening: microscopic, which gives rise to broadened Landau levels; and macroscopic, such as density fluctuations, which smears the sharp structure. If the carriers are in the 2D limit (no Landau level overlap), it is simple to separate the two contributions. In the absence of inhomogeneous broadening, the susceptibility near $B=B_N$ may be approximately written $\chi=\chi_0-\chi_1\delta(B-B_N)$, where $\delta(x)$ is a Dirac δ function, and χ_0 and χ_1 are (approximately) constants. If there is inhomogeneous broadening—say n has a distribution $P(n)$ peaked near $n=n_0$—then the spike in χ will be

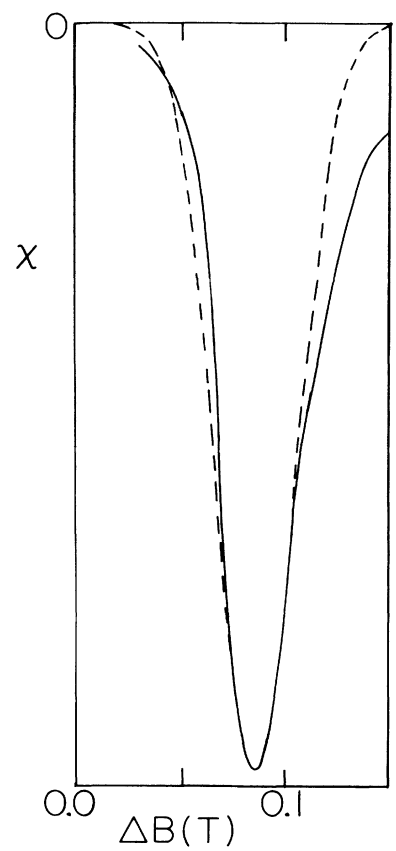

FIG. 8. Inhomogeneously broadened negative susceptibility spike. Solid line, average of several spikes of sample in Fig. 1(a), near 12 T. Dashed line, Gaussian fit with variance $\sigma/n=0.0017$, corresponding to full width at half maximum $\Delta n/n=0.40\%$.

smeared out:

$$\chi(B)=\chi_0-\chi_1 P(B) , \tag{1}$$

where $P(B)=P(n_1)$, with $n_1=NB/\Phi_0$ (recall that $\Phi_0 n_0=NB_N=F$). Figure 8 shows a composite experimental $\chi(B)$ curve, averaged over several negative spikes near $B=12$ T. The $P(n)$ function is seen to be slightly asymmetric, but approximately Gaussian [i.e., $\sim\exp-(n-n_0)^2/2\sigma^2$] with full width corresponding to a 0.40% variation in n. This is comparable to the density variations found in the low-density 2D EG systems studied.[2-6] It should be noted that any residual magnetic torque[14] would also contribute to this broadening. The same inhomogeneous broadening (Gaussian approximation) is used in the theoretical curves, Figs. 2, 5–7. A simplification is made in the calculation, however. Rather than recalculate the averaged χ for each value of B, χ was calculated for fixed $n=n_0$ for the full range of B, then broadened at each B by a Gaussian smearing of χ in $1/B$. Since χ is a function of n/B multiplied by a slowly varying function of B, the two smearing mechanisms should be equivalent. A few checks using the more time consuming n smearing showed that the two broadening functions do produce equivalent results.

D. Line-shape calculations—Landau level bandwidth

Microscopic disorder broadens the Landau level into a band, and can be incorporated through the density-of-state (DOS) function for a Landau level, $G_N(E)=G[(E-E_N)/\Gamma]$, where 2Γ is the width of the level, and G is normalized to unity

$$\left[\int_{-\infty}^{\infty} G(z)dz=1\right] .$$

Thermodynamic functions can be expressed in terms of integrals of G, summed over Landau levels.[17] For instance, $\varepsilon=\varepsilon_{\text{nonosc}}+\varepsilon_{\text{osc}}$, where only ε_{osc} contributes to dHvA oscillations. If the Landau levels are sufficiently sharp that only the two levels nearest the Fermi level $(N,N-1)$ are partially occupied (i.e., not completely full or empty), then[17]

$$\varepsilon_{\text{osc}}=\frac{-n_d B\Gamma}{\Phi_0}\left[G^{(2)}\left[\frac{E_F-(N-\frac{1}{2})\hbar\omega_c}{\Gamma}\right]+G^{(2)}\left[\frac{(N+\frac{1}{2})\hbar\omega_c-E_F}{\Gamma}\right]\right] , \tag{2a}$$

where $\partial^2 G^{(2)}(z)/\partial z^2=-\partial G^{(1)}(z)/\partial z=G(z)$, and the generalization to more than two levels is straightforward. The density is given by a similar expression:

$$n=\frac{n_d B}{\Phi_0}\left[N+G^{(1)}\left[\frac{(N+\frac{1}{2})\hbar\omega_c-E_F}{\Gamma}\right]-G^{(1)}\left[\frac{E_F-(N-\frac{1}{2})\hbar\omega_c}{\Gamma}\right]\right] . \tag{2b}$$

The factor n_d in Eq. (2) is the degeneracy of a single Landau level. In the subsequent equations, we take $n_d=2$ (due to spin) for simplicity. However, it should be noted that in graphite intercalation compounds there is an extra twofold orbital degeneracy; moreover, in the calculations used in generating the figures, a spin splitting with $g=2$ was incorporated. In the present work, M and χ have been calculated directly from the appropriate derivatives of Eq. (2a). However, if $N\gg 1$, only the derivatives of the $G^{(n)}$ functions make an important contribution, greatly simplying the expressions for M and χ. For instance, χ may be approximately written

$$\chi\cong\frac{2}{\Phi_0}\frac{(\hbar\omega_c)^2}{B\Gamma}[(N-\tfrac{1}{2})^2 G_{N-1}(E_F)+(N+\tfrac{1}{2})^2 G_N(E_F)]$$
$$\cong\frac{2nF_0}{\Gamma B}\left[\frac{\hbar\omega_c}{B}\right]^2[G_{N-1}(E_F)+G_N(E_F)] . \tag{3}$$

That is, χB is a constant times the DOS at E_F.

The calculations in Figs. 2, 5–7 incorporate the "semielliptic" DOS appropriate to collision broadening of the Landau level:[17,18]

$$G(z)=G_{\text{coll}}\equiv\frac{2}{\pi}(1-z^2)^{1/2} . \tag{4}$$

In calculating χ, it is assumed that the system is in thermal equilibrium—that is, that the interband scattering times are short enough that both light and heavy holes always have a common Fermi level, E_F. In the calculations this was done by guessing a value of E_F, calculating the light-hole density n_l and the heavy-hole density n_h separately [by Eq. (2b)], then adjusting E_F until $n_l+n_h=n_0$. It should be pointed out that spin splitting has been incorporated into the theoretical calculations, but it effects are not visible in χ for the assumed g value ($g=2$)—in accord with the experimental data.

V. GENERAL FEATURES OF M,χ

Much insight into the structure of dHvA oscillations can be gained by careful study of equations like Eqs. (2) and (3). We present two examples.

A. $M\propto E_F-E_{F0}$

In the same approximation ($N\gg 1$) used to derive Eq. (3), M may be approximated in an extremely compact form (Appendix C):

$$M\cong\frac{mE_F}{B\pi\hbar^2}(E_F-E_{F0})\cong\frac{2N+1}{\Phi_0}(E_F-E_{F0}) , \tag{5}$$

where $E_{F0}=\pi\hbar^2 n/m\equiv n/D_0$. For a single band 2D EG, E_{F0} is the zero-field value of the Fermi energy, and the sawtooth magnetization just represents the oscillations of E_F with field. For the multiband case, M is a sum of terms from each band, and E_{F0} is no longer the zero-field Fermi energy, since the carrier densities in the individual bands are not separately constant.

Equation (5) offers a lot of insight in the dHvA oscillations. As long as there is a gap between Landau levels, E_F will jump discontinuously between levels at fields

$B = B_N$, leading to jumps in M and spikes χ. Interpretation of the results of Ref. 16 is now clear. Finite temperatures or localized states in the gap will smooth out the E_F variations, and hence also the structure in M,χ.

B. χ oscillations with two hole bands

The presence of two bands causes profound changes in the dHvA oscillations. While these effects are also present in three-dimensional metals, the effects are greatly enhanced in 2D, since the Fermi energy changes much more strongly with magnetic field. The nature of the effects depends dramatically on the bandwidth of the Landau levels, as illustrated in Fig. 9. If both bands are very narrow levels [Fig. 9(a)], the bands rarely overlap. As the field increases, the Fermi level sits in the highest Landau level until it is depopulated, then jumps to the next highest level, regardless of which band it comes from. Since each band has the same degeneracy, the Fermi level stays in each Landau level for the same interval in inverse field. Hence the dHvA oscillations show a *single* frequency ($F = F_l + F_h$) corresponding to the *sum* of the carrier densities, with no trace of the individual bands. This case has been discussed in detail by Vinter and Overhauser[19] (VO). Actually, there is also a sharp peak in χ when Landau levels from both bands cross E_F simultaneously, which they do with frequency $F_h - F_l$, but VO show that this spike is washed out by inhomogeneous broadening. Figure 9(a) still shows traces of the presence of the two bands. Note that the sharpest experimental dHvA spectrum is approaching this limit. The most intense peak in the Fourier transform of Fig. 4(b) corresponds to the sum frequency, $F_l + F_h$.

In the opposite limit, when both Landau levels are broad, the dHvA oscillations are weak and sinusoidal, and do not show strong mixing frequencies. There is, however, an interesting intermediate situation: if one level is broad and the other narrow [Fig. 9(d)]. In an extreme case the heavy-hole Landau level may be so broadened out that it shows no dHvA oscillation. Its presence can still be determined by its effect on the line shape of the light-hole oscillation: the heavy holes will act as a carrier reservoir, pinning E_F, so the light-hole dHvA oscillations will just map out the light-hole DOS at E_F. Specifically, a small field change ΔB leads to $\Delta n_l = -\Delta n_h = -D_{h0}\Delta E_F$, and (Appendix C)

$$\chi = \frac{(2N+1)}{\Phi_0 B}\left[1+\frac{D_{h0}}{D_{l0}}\right]\left\{\frac{(N+\frac{1}{2})\hbar\omega_c D_l - n_l}{D_l + D_{h0}}\right\}, \qquad (6)$$

where D_{l0}, D_{h0} are the zero-field DOS and D_l is the actual light-hole DOS at E_F. If $D_{h0} \gg D_l$, χ is just proportional to D_l (up to a constant shift), as in Fig. 9(d). This figure should be contrasted to the spectrum for the same light hole band, but in the absence of heavy holes [Fig. 9(e)]. In the former case, E_F is pinned by the heavy holes between light-hole Landau levels, leading to a weak negative χ over an extended field range. In the latter case, E_F jumps between light-hole Landau levels, leading to a sharp negative spike in χ.

Figure 9 also illustrates some intermediate cases [Figs. 9(b) and 9(c)] were $\Gamma_h > \Gamma_l$. Here the two features discussed above are combined. The susceptibility shows the overall shape of Fig. 9(d): positive altering with negative over each half of the light-hole dHvA period. In the positive half period (Fermi level in a light-hole Landau level), the heavy holes make only a relatively minor perturbation in the spectrum. In the negative half period, the Fermi level is in a gap between the two light-hole levels, and is strongly modulated by the heavy holes [they have the shape of Fig. 9(e), with strong negative spikes]. This explains the unusual asymmetric spectra of Fig. 1.

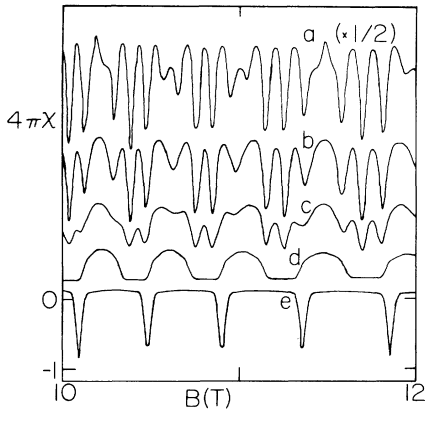

FIG. 9. Interband mixing effects in dHvA spectrum: line shape changes as the heavy-hole band is broadened out. (a), VO limit—both bands sharp ($\Gamma_l = \Gamma_h = 0.05$ meV); (b)–(d), gradual broadening of heavy holes: $\Gamma_h = 2$ meV (b), 3 meV (c), ∞ (d), while $\Gamma_l = 1.5$ meV in all; (e) $= \Gamma_l = 1.5$ meV, but no heavy holes. In all calculations, a Gaussian broadening with $\sigma/n = 0.0015$ has been incorporated.

VI. DISCUSSION OF RESULTS

Figures 1, 2, 5–7 show that the theory gives a very good description of the dHvA oscillations. The most obvious discrepancy between Figs. 1 and 2 is a small field shift (~ 0.1 T). This can be partly an experimental artifact (field calibration error plus a shift in the recorded field positions, due to sweeping the field too fast), but the field position is also very sensitive to small errors in the dHvA frequency. Considerable improvement could be made in the fit by varying the dHvA frequencies and Γ values to obtain a best fit for each spectrum. However, it was felt to be important to show how good a fit could be obtained by taking the dHvA frequencies from a Fourier transform and using common Γ values for all samples.

Since the dHvA frequencies and effective masses are independently determined, the remaining parameters can be unambiguously extracted. The inhomogeneous broadening is directly measured from the broadened line shape of the negative χ spike, as discussed above (Fig. 8). This leaves two parameters: the broadening of the light holes (Γ_l), adjusted to fit the low field data (Fig. 6), and

of the heavy holes (Γ_h), adjusted to fit Fig. 1. Interestingly, a good fit can be obtained for all samples by choosing the Γ's to be approximately field independent, and in fact, equal to each other, $\Gamma_l=\Gamma_h=1.4$ meV. While the semielliptic DOS, Eq. (4), gives a good description of the χ oscillations, theory[18] also predicts the impurity scattering should cause $\Gamma \propto B^{1/2}$, which is not observed experimentally. An alternative possibility is that the Landau level broadening is a band-structure effect due to c-axis dispersion of the electronic energy states: the Fermi surfaces are not perfect cylinders but have maximum and minimum radii differing by $2\Gamma \cong 3$ meV. In this case Γ would be expected to be field independent and, moreover, $\Gamma_l \cong \Gamma_h$ (Appendix A). The value of Γ is comparable to that found in $SbCl_5$-GIC.[20] The bandwidth can also be estimated from the conductivity anisotropy[12] and for Br_2 GIC a value $\Gamma \cong 3.5$ meV was found. This is only an upper limit, since the c-axis band conductivity can be enhanced by hopping conduction.[21] However, c-axis dispersion should produce a very different DOS. If $E=E(k_\rho)+\Gamma\cos(I_c k_z)$, where I_c is the c-axis repeat distance, then the DOS is that appropriate to a one-dimensional band $G(z)\propto(1-z^2)^{-1/2}$. This DOS has singularities at both upper and lower band edges, which should show up in χ (Fig. 10). Figure 10 shows that in an ideally sharp spectrum, it is relatively easy to distinguish the density of states: contrast Figs. 10(a) and 9(d). However, with realistic broadening, the singularities produce only a small splitting of the dHvA peaks. It is possible that this too could be washed out if impurity scattering distorts the DOS. While we have occasionally observed this kind of peak splitting (see Fig. 7), it will require more work to see if it is reproducible and also whether it might instead be associated with spin splitting.

From the values of Γ, the fields B_{2D} can be derived (Table I), where B_{2D} is the field above which successive Landau levels no longer overlap:

$$\frac{\hbar e B_{2D}}{mc}=2\Gamma \ . \tag{7}$$

Comparing Table I and Fig. 5, it can be seen that the heavy-hole oscillations first become prominent near B_{2Dh}. This field, B_{2Dh}, is important, since above this field, the hole gas behaves fully two dimensionally and, in principle, a quantum Hall effect should be observable.[22,23] We conclude with a number of observations.

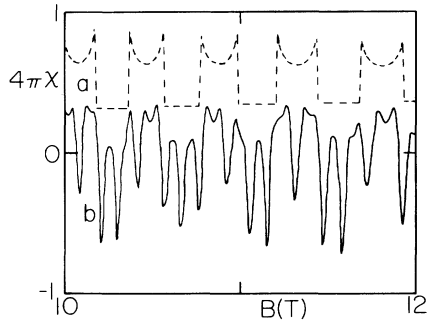

FIG. 10. Theoretical dHvA oscillations assuming a DOS appropriate to one-dimensional band dispersion. (a): $\Gamma_l=1.5$ meV, $\Gamma_h=\infty$, no Gaussian broadening [to be compared with Fig. 8(d)]. (b): $\Gamma_l=\Gamma_h=1.5$ meV, $\sigma/n=0.0015$. (Spin splitting neglected in these calculations.)

From the (theoretical) amplitude, it is found that $4\pi\chi \leqq 0.6$ for all B fields, suggesting that Condon domain formation ($4\pi\chi>1$) is unlikely in Br_2-GIC. However, Shoenberg[24] has shown that inhomogeneous broadening will not affect the local formation of Condon domains, so Condon domain formation might be possible in the field range 3–4 T, where the unbroadened $4\pi\chi>1$. Condon domain formation should be more readily observed in a number of other acceptor GIC, which have larger Fermi surface areas, but still should have[12] $\Gamma \cong 1$ meV.

The above calculations do not introduce a Dingle temperature, such as is common in three-dimensional analyses of the dHvA effect (see discussion in Ref. 17). If, however, there were a small Dingle temperature (say $k_B T_D=h/\tau$, with τ the conductivity scattering rate) its effect would be negligible in comparison to the DOS and inhomogeneous broadening mechanisms discussed above.

The inhomogeneous broadening discussed above produces a smearing of the dHvA oscillations proportional to B [see Eq. (1)]. It might be imagined that the same dHvA line shape would be produced by ignoring inhomogeneous broadening, but introducing a DOS linewidth Γ proportional to B. While this is qualitatively correct, we have not been able to reproduce the detailed line shape with such a model [see Fig. 3(a)]. The observation of a sample [Fig. 1(e)] with substantially reduced inhomogeneous broadening, but the same values of Γ, lends support to the present interpretation, and suggests that with better control over sample preparation, even more nearly ideal samples can be prepared.

ACKNOWLEDGMENTS

This research is supported by U.S. Air Force Office of Scientific Research (AFOSR) Grant No. F49620-82-C-0076. The National Magnet Laboratory is supported at Massachusetts Institute of Technology by the National Science Foundation. We thank D. Shoenberg for extremely useful conversations and A. W. Moore for the HOPG samples. The x-ray studies were done in collaboration with D. Chipman.

APPENDIX A: PROPERTIES OF GIC ENERGY BANDS

1. Effective mass

It was shown in Ref. 13 that, for any stage 2 GIC, the dHvA frequencies could be approximately written

$$F_\pm=\frac{\Phi_0}{3\pi a_0^2}\frac{E_F(E_F\pm\gamma_1)}{(\gamma_0\pm\gamma_4)^2} \ , \tag{A1}$$

where $a_0=2.46$ Å, the γ_i are graphitic band parameters, with approximate values[25] $\gamma_0=3$ eV, $\gamma_1\cong 0.39$ eV, $\gamma_4\cong 0.18$ eV, and the subscript $+(-)$ refers to light (heavy) holes ($E_F<0$ for holes). Moreover, the effective

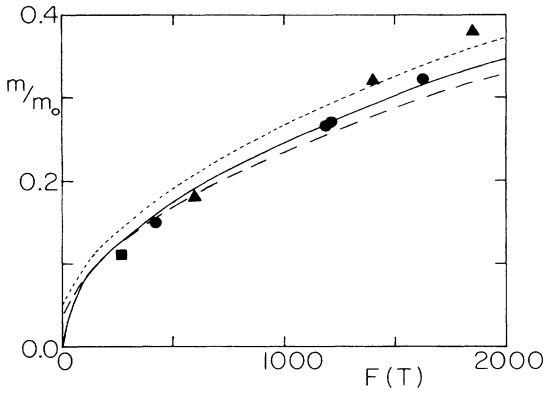

FIG. 11. Effective mass vs dHvA frequency F for acceptor GIC of stage 1 (solid line) and stage 2 (long dashes, light holes; short dashes, heavy holes). Data: square, Br_2 (present work); triangle, AsF_5 (Refs. 13 and 28); and circle, $SbCl_5$ (Ref. 26).

masses can be written

$$\frac{m_\pm}{m_0}=\frac{2\hbar^2}{3m_0a_0^2}\frac{|2E_F\pm\gamma_1|}{(\gamma_0\pm\gamma_4)^2}\ . \tag{A2}$$

where m_0 is the free electron mass. This leads to a *universal relation:*

$$\frac{m_\pm}{m_0}=\frac{4\hbar^2}{m_0a_0(\gamma_0\pm\gamma_4)}\left[\frac{\pi(F+F_x)_\pm}{3\Phi_0}\right]^{1/2}, \tag{A3}$$

where

$$F_{x\pm}=\frac{\Phi_0}{12\pi a_0^2}\left[\frac{\gamma_1}{\gamma_0\pm\gamma_4}\right]^2. \tag{A4}$$

A similar equation holds for a stage-1 compound (one graphite layer per intercalant layer hence only one hole band), with $\gamma_1=\gamma_4=0$. Since $\gamma_0\gg\gamma_1,\gamma_4$, this expression is almost stage independent, but is found to consistently underestimate the observed values.[13,26] The agreement can be improved either by decreasing the value of γ_0 (to about 2.6 eV) (Ref. 26) or by incorporating an electron-phonon mass enhancement factor[13,27] λ_{ep} [so the right-hand side of Eq. (A3) is multiplied by $1+\lambda_{ep}$]. Figure 11 shows a comparison between the data,[13,26,28] and Eq. (A3), corrected with $\lambda_{ep}=0.18$. (The data suggest that λ_{ep} might depend slightly on F, varying from 0.14 to 0.20–0.34 for the highest point—as F increases.) The observed values $F_+=262$ T, $F_-=900$ T, give $E_F=-0.822$ eV, $\gamma_1=0.377$ eV (assuming γ_0,γ_4 as above). Using these values in the corrected Eq. (A3) gives effective masses of 0.127, 0.252.

2. Nonparabolicity

Equations (A1) and (A2) represent highly nonparabolic energy bands. In a strong magnetic field, they lead to the following semiclassical quantization condition[29] (where the small parameter γ_4 is set equal to zero):

$$E\left[1\mp\frac{E}{\gamma_1}\right]=\mp E'_N=\mp(N+\tfrac{1}{2})\hbar eB/m'c\ , \tag{A5}$$

where $m'=2\hbar^2\gamma_1/3a_0^2\gamma_0^2$. The effects of nonparabolicity on the magnetization may readily be found, following the technique of Ref. 30. Using the DOS integrals of Eq. (2), it is found that

$$G_{np}^{(1)}(E)=G_p^{(1)}(E^*)\ ,$$

$$G_{np}(E)=(1\mp 2E/\gamma_1)G_p(E^*)\ ,$$

where $E^*=E(1\mp E/\gamma_1)$ and the subscript $(n)p$ stands for (non)parabolic. Using just the first term in Eq. (2a), for illustrative purposes, $M_{\rm osc}=-d\varepsilon_{\rm osc}/dB$ can be written

$$M_{\rm osc,np}=\frac{\pm 2E'_{N-1}}{\Phi_0}\int_{-\infty}^{E}G_p\left[\frac{E^*\pm E'_{N-1}}{\Gamma}\right]dE$$

$$=\pm\frac{2E'_{N-1}}{\Phi_0}\int_{-\infty}^{E^*}\frac{G_p\left[\dfrac{E^*\pm E'_{N-1}}{\Gamma}\right]dE^*}{1\mp 2E/\gamma_1}\ . \tag{A6}$$

Since $|E-E_F|\leq 2\Gamma\ll\gamma_1$, the denominator in the integrand of Eq. (A6) may be approximated by $1\mp 2E_F/\gamma_1$, and taken outside the integral, yielding

$$M_{\rm osc,np}=\frac{M'_{\rm osc,p}}{2E_F/\gamma_1\pm 1}\ , \tag{A7}$$

where $M'_{\rm osc,p}$ is the oscillatory magnetization of a parabolic band of mass m'. If the Fermi level is adjusted so that $M'_{\rm osc,p}$ gives the correct periodicity in field, then $M'_{\rm osc,p}\propto 1/m'$. Hence $M_{\rm osc,np}$ is the same as M for a parabolic band with mass $m=m'(2E_F/\gamma_1\pm 1)$. But this is the same as given by Eq. (A2) (recall that γ_4 has been set equal to zero). To summarize, to calculate M for a nonparabolic band, calculate it for a parabolic band with the correct effective mass, with E_F adjusted to give the correct field periodicity. The only error introduced will be that in going from Eq. (A6) to Eq. (A7), which is of order $2\Gamma/(2E_F\pm\gamma_1)\ll 1$. This is the procedure followed in this paper.

As noted above, the true nonparabolic $E_F=-0.822$ eV, with band splitting $\bar{\Delta}=\gamma_1=0.379$ eV. To give the correct dHvA frequencies, the parabolic fit uses $\bar{\Delta}=0.18$ eV, and finds a field dependent E_F averaging -0.477 eV.

3. *c*-axis bandwidth

The calculations of Ref. 12 are for stage-1 compounds. While the overlap integrals connecting carbon layers across the intercalant layer should be stage independent, it is not immediately clear what are the relative bandwidths of the heavy and light holes. This appendix briefly summarizes such a calculation, which shows that the two bands have comparable c-axis dispersion.

If there is no energy overlap across the intercalant layer, the energy bands are strictly two dimensional, and are determined by the Slonczewski-Weiss-McClure[31] Hamiltonian restricted to two layers:

$$\det\begin{bmatrix} \Delta-E & -\gamma_0\sigma^* & -\gamma_1 & \gamma_4\sigma \\ -\gamma_0\sigma & -E & -\gamma_4\sigma & \gamma_3\sigma^* \\ -\gamma_1 & -\gamma_4\sigma^* & \Delta-E & \gamma_0\sigma \\ \gamma_4\sigma^* & \gamma_3\sigma & \gamma_0\sigma^* & -E \end{bmatrix}=0 , \tag{A8}$$

where $\sigma=\sqrt{3}a_0ke^{i\alpha/2}$, Δ and the γ's are energy integrals, k is the in-plane wave vector, and α the angle it makes with the graphite [100] direction. Overlap across the intercalant layer couples successive graphite sandwiches, producing c-axis dispersion. This can be incorporated in Eq. (A8) by the substitutions

$$\gamma_1\rightarrow\gamma_1+\overline{\gamma}_1e^{-iQ}$$

$$\gamma_4\sigma\rightarrow\gamma_4\sigma-\overline{\gamma}_4\sigma^*e^{-iQ}$$

$$\gamma_3\sigma\rightarrow\gamma_3\sigma+\overline{\gamma}_3\sigma^*e^{iQ} ,$$

where $Q=k_zI_c$ and $\overline{\gamma}_1,\overline{\gamma}_3,\overline{\gamma}_4$ are the symmetry-allowed overlap integrals. To find approximate solutions to Eq. (A8) corresponding to Eq. (A1), a number of terms can be omitted: Δ, because it produces only a very small shift; γ_3, because it produces only a trigonal warping of the Fermi surface without changing the area,[13] and the terms higher than linear in small parameters $\overline{\gamma}_1$ and $\overline{\gamma}_4$. Then $\overline{\gamma}_4$ can be neglected, as producing only a warping of the Fermi surface, and the solutions, Eq. (A1), are recovered except for the substitution

$$\gamma_1\rightarrow\gamma_1+\overline{\gamma}_1\cos Q . \tag{A9}$$

This yields $F_\pm=F_\pm^{(0)}\mp(\delta F_\pm)\overline{\gamma}_1\cos Q$, where $F_\pm^{(0)}$ is given by Eq. (A1). The correction factors are in the ratio $\delta F_+:\delta F_-:\delta F_1=0.89:1.13:2$ (where δF_1 is the correction factor for stage 1). Hence the bandwidth in stage 2 is about half the stage-1 bandwidth. This can be seen in the data displayed in Ref. 12. Note that, as found experimentally, both bands have approximately the same width.

APPENDIX B: AMPLITUDE OF SUSCEPTIBILITY OSCILLATIONS

If the drive coil is of length l_1, diameter d_1, and has a total of N_1 turns, then an ac current I in the coil will produce an ac magnetic field B_1 at the center of the coil, where

$$B_1=\frac{\mu_0N_1I}{(l_1^2+d_1^2)^{1/2}} . \tag{B1}$$

Typical values are $d_1=2.55$ cm, $l_1=4.5$ cm, $N_1=400$, $I=10$ mA, so $B_1\cong1G$—the field B_1 is always $\leqq10G$ and hence much less than the dc field.

This field induces an ac magnetic moment in the sample

$$\mu=4\pi\chi B_1V_0 , \tag{B2}$$

where V_0 is the sample volume (~0.1 cm^3). This time varying moment induces a voltage in the pickup coil. If the pickup coil has length l_2, diameter d_2, and N_2 turns, then a point dipole would induce a voltage

$$V=\frac{N_2\omega\mu}{(l_2^2+d_2^2)^{1/2}} , \tag{B3}$$

where ω is the ac frequency. Typically, $d_2=1.6$ cm, $l_2=2$ cm, $N_2=860$, so

$$4\pi\chi\cong0.5V/f , \tag{B4}$$

where V is in mV and f is the frequency in kHz.

There are corrections to Eqs. (B1) and (B3), but they should be small. For balancing the two secondary coils, the sample is off center of the drive coil, leading to a multiplicative correction to the right-hand side (rhs) of (B1) equal to $\eta_1\cong0.92$. Also, the sample is not a point dipole. By replacing the sample by a circular current loop of the same magnetic moment and cross-sectional area, the mutual induction may be calculated exactly, leading to an extra correction of the rhs of (B3) by $\eta_2=1.03$.

The amplitude of the oscillation estimated from the pickup voltage, using the above procedure, is typically found to be no more than half of the theoretical value. For instance, the sample of Figs. 1(c), 5, and 6—the only one for which eddy current corrections could easily be made—shows an amplitude only 33% of theory. The reason for this discrepancy is not understood. It suggests that the samples are not perfectly intercalated. This is consistent with our observation that the intensity per unit volume shows large sample-to-sample variations. It should be noted that the theoretical value of χ is for noninteracting electrons, whereas some calculations[32] of Coulomb interaction effects suggests that the amplitude of χ could be substantially reduced at these carrier densities. However, the most recent calculation[33] shows no such reduction.

APPENDIX C: DERIVATION OF EQS. (5) AND (6)

The calculations described in this manuscript are an extension of Shoenberg[17] to a two-band case. Shoenberg's notation was altered to avoid doubly defining the same symbols: $F\rightarrow G^{(1)}$; $E\rightarrow G^{(2)}$. In this appendix, I briefly sketch the derivation of Eqs. (5) and (6). It should be stressed that these are approximations, use to clarify the understanding of the magnetization and susceptibility line shapes, but the full expressions for M and χ were used in all the actual calculations, which generated the figures. In what follows, equations quoted directly from Shoenberg[17] are identified by a prefactor S. Note carefully the logic: experimentally the density n (Shoenberg's N) is fixed, but the calculation is done *for fixed* E_F, and finally E_F is adjusted to give the correct n. Hence M is given by Eq. (S20). As is usual in a de Haas-van Alphen studies when many Landau levels are occupied—the Landau level index N (Shoenberg's n) $\gg1$—only the derivatives with respect to the oscillatory function are important. Hence the terms in $G^{(2)}$ can be neglected in (S20), as can $\frac{1}{2}\ll N$. Hence the terms in $G^{(1)}$ can be rewritten in terms of the density n, Eq. (S21), so Eq. (S20) becomes

$$M=\frac{2N+1}{\Phi_0}\left[E_F-\frac{n\Phi_0\hbar\omega_c}{2B}\right], \tag{C1}$$

which is equivalent to Eq. (5).

Equation (6) applies only to the special case of Fig. 9(d): there are two hole bands, but the heavy holes are so broadened out that they provide only a background density, tending to pin the Fermi level, with no oscillations. Hence only the oscillatory susceptibility of the light holes need be calculated. Equation (C1) may be used for the light-hole contribution only, and to calculate $\chi=\partial M/\partial B$ requires both $\partial E_F/\partial B$ and $\partial n_l/\partial B$.

Consider what happens when the field increases by ΔB, if the Fermi level is in the Nth light-hole level. The change in E_F can be divided into two parts. If E_F stayed fixed with respect to the bottom of the Landau level, it would shift in absolute terms because of the Landau level shift with B:

$$\Delta E_{F1}=(N+\tfrac{1}{2})\hbar\omega_c\,\Delta B/B\ . \tag{C2}$$

This increases n_l, because the degeneracy of each level is proportional to B:

$$\Delta n_{l1}=n_l\,\Delta B/B\ . \tag{C3}$$

To compensate for this change, E_F can also shift with respect to the Landau level edge by an amount ΔE_{F2}, producing a change in n_l of

$$\Delta n_{l2}=D_l\,\Delta E_{F2}\ . \tag{C4}$$

The total shift of E_F, $\Delta E_F=\Delta E_{F1}+\Delta E_{F2}$, produces a change of the heavy-hole density

$$\Delta n_h=D_{h0}\,\Delta E_F\ , \tag{C5}$$

where D_{h0} is, by assumption, field independent. But the total charge density is conserved, so $\Delta n_l+\Delta n_h=0$, or

$$\Delta n_{l2}=-(D_{h0}\,\Delta E_F+n_l\,\Delta B/B)\ ,$$

so

$$\Delta E_F=(N+\tfrac{1}{2})\hbar\omega_c\frac{\Delta B}{B}-\frac{1}{D_l}\left[D_{h0}\,\Delta E_F+\frac{n_l\,\Delta B}{B}\right],$$

or

$$\frac{\Delta E_F}{\Delta B}=\frac{D_l}{D_l+D_{h0}}\left[(N+\tfrac{1}{2})\hbar\omega_c-\frac{n_l}{D_l}\right]/B\ . \tag{C6}$$

Also

$$\frac{\Delta n_l}{\Delta B}=-D_{h0}\frac{\Delta E_F}{\Delta B}\ . \tag{C7}$$

Hence, taking a derivative of Eq. (C1) yields

$$\chi=\frac{2N+1}{\Phi_0}\left[1+\frac{D_{h0}}{D_{l0}}\right]\frac{\partial E_F}{\partial B}\ , \tag{C8}$$

where $D_{l0}=2B/\Phi_0\hbar\omega_c=m_l/\pi\hbar^2$. Substituting (C6) into (C8), yields Eq. (6).

[1]K. von Klitzing, G. Dorda, and M. Pepper, Phys. Rev. Lett. **45**, 494 (1980).

[2]E. Gornik, R. Lassnig, G. Strasser, H. L. Stormer, A. C. Gossard, and W. Wiegmann, Phys. Rev. Lett. **54**, 1820 (1985).

[3]J. P. Eisenstein, H. L. Stormer, V. Narayanamurti, A. Y. Cho, A. C. Gossard, and C. W. Tu, Phys. Rev. Lett. **55**, 875 (1985).

[4]T. P. Smith, III, B. B. Goldberg, P. J. Stiles, and M. Heiblum, Phys. Rev. B **32**, 2696 (1985).

[5]E. Stahl, D. Weiss, G. Weimann, K. von Klitzing, and K. Ploog, J. Phys. C **18**, L783 (1985).

[6]M. G. Gavrilov and I. V. Kukushkin, Pis'ma Zh. Eksp. Teor. Fiz. **43**, 79 (1986); I. V. Kukushkin and V. B. Timofeev, *ibid.* **43**, 387 (1986).

[7]In contrast to Refs. 2–6, F. Fang and P. W. Stiles [Phys. Rev. B **28**, 6992 (1983)] observed sharp susceptibility spikes suggestive of a true energy gap. However, it was suggested in Refs. 3 and 8 that this was really an eddy current effect.

[8]V. M. Pudalov, S. G. Semenchinsky, and V. S. Edelman, Solid State Commun. **51**, 713 (1984).

[9]M. S. Dresselhaus and G. Dresselhaus, Adv. Phys. **30**, 139 (1981).

[10]I. D. Vagner, T. Maniv, and E. Ehrenfreund, Phys. Rev. Lett. **51**, 1700 (1983).

[11]R. S. Markiewicz, Phys. Rev. B **34**, 4172 (1986); **34**, 4177 (1986); **34**, 4183 (1986).

[12]R. S. Markiewicz, Solid State Commun. **57**, 237 (1986).

[13]R. S. Markiewicz, Solid State Commun. **44**, 791 (1982).

[14]D. Shoenberg, *Magnetic Oscillations in Metals* (University Press, Cambridge, 1984); J. Vanderkooy and W. R. Datars, Can. J. Phys. **46**, 1215 (1968); and R. S. Markiewicz, Y. P. Ma, J. D. Nettinger, and J. S. Brooks (unpublished).

[15]R. S. Markiewicz, M. Meskoob, and C. Zahopoulos, Phys. Rev. Lett. **54**, 1436 (1985) and R. S. Markiewicz, M. Meskoob, and C. Zahopoulos, Synth. Met. **12**, 359 (1985).

[16]I. D. Vagner and T. Maniv, Phys. Rev. B **32**, 8398 (1985).

[17]D. Shoenberg, J. Low Temp. Phys. **56**, 417 (1984).

[18]T. Ando and Y. Uemura, J. Phys. Soc. Jpn. **36**, 959 (1974).

[19]B. Vinter and A. W. Overhauser, Phys. Rev. Lett. **44**, 47 (1980).

[20]H. Zaleski and W. R. Datars, Bull. Am. Phys. Soc. **31**, 643 (1986).

[21]K. Sugihara, Phys. Rev. B **29**, 5872 (1984).

[22]M. Ya. Azbel, Phys. Rev. B **30**, 2273 (1984).

[23]H. L. Stormer, J. P. Eisenstein, A. C. Gossard, W. Wiegmann, and K. Baldwin, Phys. Rev. Lett. **56**, 85 (1985).

[24]D. Shoenberg, J. Low Temp. Phys. **25**, 755 (1976).

[25]L.G. Johnson and G. Dresselhaus, Phys. Rev. B **7**, 2275 (1973); the smaller value chosen for γ_0 is in accord with optical studies: D. M. Hoffman, P. C. Eklund, R. E. Heinz, P.

Hawrylak, and K. R. Subbaswamy, Phys. Rev. B **31**, 3973 (1985).

[26]H. Zaleski, P. K. Ummat, and W. R. Datars, J. Phys. C **17**, 3167 (1984).

[27]F. Guinea, J. Phys. C **14**, 3345 (1981).

[28]Reference 13 found an anomalously large heavy-hole mass in a stage-2 AsF_2-GIC. Figure 7 reports more recent data on a lower density compound. The reason for the mass anomaly is not known, although it may be related to magnetic breakdown of an in-plane superlattice.

[29]M. Inoue, J. Phys. Soc. Jpn. **17**, 808 (1962).

[30]M. Kubisa and W. Zawadzki, Solid State Commun. **59**, 339 (1986).

[31]J. C. Slonczewski and P. R. Weiss, Phys. Rev. **109**, 272 (1958); J. W. McClure, Phys. Rev. **108**, 612 (1957).

[32]N. J. M. Horing and J. J. LaBonney, J. Mag. Mag. Mats. **11**, 73 (1979); A. Isihara and Y. Shiwa, in *Proceedings of the 17th International Conference of Low Temperature Physics,* edited by U. Eckern, A. Schmid, W. Weber, and H. Wühl (Elsevier, Amsterdam, 1984), p. 871.

[33]A. H. MacDonald, H. C. A. Oji, and K. L. Liu, Phys. Rev. B **34**, 2681 (1986).